More dynamic than expected: An updated survey of surging glaciers in the Pamir

Franz Goerlich[1], Tobias Bolch[2], Frank Paul[1]

[1]Department of Geography, University of Zurich, Zurich, Switzerland
[2]School of Geography and Sustainable Development, University of St. Andrews, St. Andrews, United Kingdom

Correspondence to: Franz Goerlich (franz.goerlich@geo.uzh.ch)

Abstract. The investigation of surging glaciers using remote sensing has recently seen a strong increase as freely available satellite data and digital elevation models (DEMs) can provide detailed information about surges that often take place in remote and inaccessible regions. Apart from analysing individual surges, satellite information is increasingly used to collect valuable data on surging glaciers. Related inventories have recently been published for several regions in High Mountain Asia including the Karakoram, parts of the Pamir and western Kunlun Shan, but information for the entire Pamir is solely available from a historic database listing about 80 glaciers with confirmed surges. Here we present an updated inventory of confirmed glacier surges for the Pamir that considers results from earlier studies and is largely based on a systematic analysis of Landsat image time series (1988 to 2018), very high-resolution imagery (Corona, Hexagon, Bing Maps, Google Earth) and DEM differences. Actively surging glaciers were identified from animations and flicker images (e.g. terminus advances) and the typical elevation change patterns. Selected historic (Corona and Hexagon) and contemporary very high-resolution imagery (Bing Maps and Google Earth) were used to confirm surges. In total, we identified 206 spatially distinct surges within 186 glacier bodies, mostly clustered in the northern and central part of the Pamir. Where possible, minimum and maximum glacier extents were digitized, but often interacting tributaries made a clear separation challenging. Most surging glaciers (n=70) are found in the larger size classes (>10 km²), but two of them are very small (<0.5 km^2). We found also several surges where the length of the glacier increased by more than 100%. The created datasets are available at: https://doi.pangaea.de/10.1594/PANGAEA.914150 (Goerlich et al., 2020).

1 Introduction

The investigation of surging glaciers using satellite data has ~~received~~ recently increased attention among scientists, in particular for the Karakoram mountain range but also other regions of the world (e.g. Berthier and Brun, 2019; Bhambri et al., 2017; Bolch et al., 2017; Falaschi et al., 2018; Minora et al., 2016; Paul, 2015 and 2020; Quincey et al., 2015; Rankl and Braun, 2016; Round et al., 2017; Steiner et al., 2018). This has several reasons, for example (a) the free access to long (Landsat) and dense (TerraSAR-X / TanDEM-X, Sentinel-1/2) time series of high-resolution satellite data, (b) the limited understanding of why some glaciers in this region are surging while others do not, (c) a large number of on-going surges at any point in time, (d) the large variations of surge behaviour in a small region, (e) the long history of still occurring surge-related hazards (mostly due to damming of a river and related outburst of lakes), and (f) the very difficult field access. Thereby, most studies

document the variations in glacier extent / length changes, flow velocities and elevation / mass changes in the course of a surge or surge-related hazards. These studies have revealed unprecedented details about surge dynamics and variations that already helped in improving our understanding of related surge mechanisms.

In contrast, the surging glaciers in the Pamir mountain ranges to the north of the Karakoram received less attention, but recently some studies were published (e.g. Lv et al. 2019; Osipova 2015; Wendt et al. 2017; Holzer et al. 2016). This might be due to the fact that several surges during the Soviet era have already been described in detail (e.g. the surges of Medvezhy and Geographical Society glaciers are well documented, see Dolgushin and Osipova (1971, 1975), Kotlyakov et al. (2003) and Osipova (2015)) and a detailed inventory describing a high number (>800) of surge-type glaciers based on satellite data and aerial images was published (Osipova et al. 1998). However, this and many of the publications are in Russian and are therefore little known internationally.

When speaking about surging glaciers, we first have to differentiate between surge-type glaciers and other glaciers. This is important when interpreting glacier changes in the context of climate change, e.g. their length or mass changes over a time period when surges have occurred (Bolch et al., 2017; Brun et al., 2017; Gardelle et al., 2013). Secondly, it is also important to distinguish surge-type from surging glaciers. The former have surged at some point in the past and show indirect evidences like looped or distorted moraines or post-surge down-wasting features of a former surge, whereas the latter surged actively within the observation period. Looped or otherwise distorted moraines occur due to former surges that pushed the lobate-shaped boundaries of tributaries downward indicate different flow speeds among major, moraine-separated glacier branches (Herreid and Truffer, 2016; Meier and Post, 1969). The typical post-surge down-wasting features are separated lower glacier parts and/or the jagged boundary of a stagnant and rapidly lowering glacier tongue, among others (Paul, 2020). We here only investigate glaciers that have actively surged during the observation period. The globally most complete compilation of surge-type glaciers by Sevestre and Benn (2015) is a most valuable starting point, but it is based on literature sources up to the year 2013 only. In the meantime, numerous further surge-type glaciers have been identified across High Mountain Asia (HMA) from the analysis of multi-temporal satellite imagery, e.g. in the Karakoram (Bhambri et al., 2017), Kunlun Shan (Yasuda and Furuya, 2015), central Tibet (Zhang et al., 2018), eastern Pamir (Lv et al., 2019) and Tian Shan (Mukherjee et al., 2017), but an update of confirmed surges for the entire Pamir Mountains is yet missing. With this study we aim at identifying them and provide detailed information (e.g. timing and typology) about confirmed glacier surges in the Pamir Mountains.

Surge-type glaciers in particular are included in the inventory by Osipova et al. (1998) and Sevestre and Benn (2015). There are thus important differences in our approach compared to the methodology used for the 'catalogue' by Osipova et al. (1998), implying that both are not directly comparable: (i) our satellite image time series (Landsat) has a lower spatial resolution (30 m) than the KFA1000 data (3-5 m) used by Osipova et al. (1998), (cf. also Dowdeswell et al. 1993, 1995), (ii) we cover a different period (1988–2018) than Osipova (1998), have (iii) used different indicators for surge identification (e.g. animations, DEM difference patterns), (iv) assigned only one surge class instead of six, and (v) our glacier entities have different boundaries as we used the most recent Pamir glacier inventory by Mölg et al. (2018) as a base for the analysis (here named GI-1).

75

The information from Osipova et al. (1998) is also available in the Randolph Glacier Inventory (RGI) version 6 (RGI Consortium 2017) using the simplified classification scheme developed by Sevestre and Benn (2015). We have used the RGI dataset and revisited existing literature, e.g. ~~and~~ the study by Lv et al. (2019), as a starting point for our inventory of glacier surges. Our analysis is primarily based on animated multi-temporal (1988-2018) time-series of Landsat data, but also on elevation difference maps showing the typical mass transfer pattern of glacier surges. For some less clear cases, we also analysed very high-resolution images from the Corona and Hexagon missions and the images in Google Earth and Bing Maps for confirmation.

For this study, we revisited the GI-1 inventory by adding ice divides for glacier units that surged but were so far connected with other glaciers in GI-1, resulting in a new inventory GI-2. In a second step, three inventory subsets are created from GI-2 that provide (a) the selection of surging glaciers only (GI-3), (b) minimum (GI-3min), and (c) maximum (GI-3max) extents of all surging glaciers. In the following, the number in brackets after a glacier's name refers to its ID in the GI-3min inventory. We also present a rough classification of the different surge-types, the timing of surges during the observation period (1988-2018), a comparison of geomorphometric characteristics (other glaciers in GI-2 vs. GI-3), a description of geometric changes due to a surge.

2 Study region

The Pamir is one of highest mountain ranges within HMA and of the world extending from about 36°35' to 39°35' N and 70°35' to 75°35' E (Fig. 1). The northern part belongs to the Osh region of Kyrgyzstan, the eastern parts to the Xinjiang Uighur Autonomous Region of China, the most southern regions to Badakhshan in northeastern Afghanistan and the main part to Gorno-Badakhshan in Tajikistan. The highest peak (Mt. Kongur) reaches up to 7649 m a.s.l. and enthrones over the Kongur Shan in the eastern part of the Pamir (all names are based on selected transliterated Russian topographic maps at a 1:500.000 and 1:100.000 scale).

Figure 1

Typical glaciers in the Pamir are long and dendritic or multi-basin valley glaciers, but other types such as mountain glaciers and cirques exist as well. Due to the steep and ice-free surrounding rock walls, most glaciers are at least partly debris covered, which often simplifies the identification of typical surge marks (e.g. looped moraines) from space (e.g. Kotlyakov et al. 2008). Most glaciers are concentrated in the central part around Ismoil Somoni Peak (7495 m a.s.l.) including Fedchenko Glacier, which is with a length of >70 km the longest valley glacier in the world outside the polar regions (Machguth and Huss, 2014). Additionally, the region is home ~~of~~ abundant rock glaciers that are not always clearly separable from debris-covered glaciers and other ice-debris landforms (Mölg et al., 2018).

The glaciers in the western and central part of the Pamir (Tadjik, Kyrgyz and Afghan regions) are of winter accumulation type where most precipitation (~90%) falls between December and May (Maussion et al., 2014)

112 with annual amounts of up to 1285 mm a^{-1} at Fedchenko weather station at 4169 m.a.s.l. (Finaev et al., 2016).
113 Conversely, the glaciers in the eastern part are mainly (50 to 60%) fed by precipitation in the summer months
114 between June and August, which can be seen as an effect of the monsoon (Maussion et al., 2014). The total
115 annual precipitation is very low in some regions, reaching only ~70 mm a^{-1} at Murgab (3576 m a.s.l.) and
116 Toxkargan weather stations, both located in valleys (3090 m a.s.l.) (Finaev et al., 2016). Hence, the glaciers in
117 the western and central part are situated in a somewhat warmer and more humid climate whereas the eastern
118 ranges are dry and cold. Accordingly, glacier mean elevations of the former can be found at lower altitudes
119 (~4740 m a.s.l.) than in the eastern regions (~5050 m a.s.l.) according to the dataset presented by Mölg et al.
120 (2018).

121

122 The likely best-investigated glacier in the region is Fedchenko (Lambrecht et al., 2014, 2018) that is so far
123 considered as not surging. Of the glaciers with confirmed surges, Medvezhy Glacier (29) is likely the best
124 investigated (see Kotlyakov et al., 2008). This latter study also reported details about surges of several other
125 glaciers in the region, partly back to 1959.

3 Datasets and pre-processing

3.1 Satellite data

3.1.1 Landsat

129 For the detection of glacier surges and determination of surge start, end and possibly their full surge cycle (e.g.
130 from the starting year of an active phase to the start of the next active phase), we used freely available Landsat
131 imagery (Level 1T) from earthexplorer.usgs.gov including Landsat 5 TM (Thematic Mapper), Landsat 7 ETM+
132 (Enhanced Thematic Mapper plus) and Landsat 8 OLI (Operational Land Imager) sensors. Additionally, we used
133 some very good scenes (no snow outside glaciers) from Landsat MSS (Multispectral Scanner) from the 1970s
134 and 1980s. The three sensors TM, ETM+ and OLI acquire data with a horizontal resolution of 30 m for the
135 visible, near-infrared (NIR) and shortwave infrared (SWIR) bands at a repeat rate of 16 days. Key characteristics
136 of the datasets are shown in Table 1, the full list of scenes used for this study is presented in Table S1 in the
137 Supplementary Material.

138

139 In general, cloud-free scenes from the end of the summer (July to October) are used from all sensors, but for
140 some regions, also earlier acquisitions are considered to have images available for as many years as possible.
141 With a focus on the changes near the glacier terminus, the remaining seasonal snow at higher elevations in these
142 images was unproblematic. Unfortunately, it was not possible to find suitable scenes for each year in most
143 regions so that the determination of the onset or end of a surge has at least a ±1 year uncertainty. Priority was
144 given to Landsat 5 TM scenes to limit using Landsat 7 ETM+ scenes after 2002 when the Scan Line Corrector
145 (SLC) stopped working (resulting in so-called SLC-off scenes). For the animations we downloaded the standard
146 colour-balanced and orthorectified image quicklooks from earthexplorer.usgs.gov that are provided in false-
147 colours (glacier ice and snow is depicted in cyan) and at the original resolution. The jpg-compression of these
148 images results locally in blurred details but they had only a very small impact on surge identification.

149

150 *Table 1*

151

3.1.2 Corona and Hexagon

153 The Corona Keyhole (KH) 4B scenes from August 1968 (Table S1) cover the central and northern Pamir (see
154 Fig. 1) and were also downloaded from earthexplorer.usgs.gov. The Corona images are panchromatic, recorded
155 in stereo mode and have a ground resolution of up to 1.8 m (Galiatsatos, 2009). We processed 11 scene pairs to
156 generate a DEM and corresponding orthophotos with 5 m resolution following Goerlich et al. (2017). Due to the
157 high effort of processing the scenes, the orthoimages only cover the region with the most surging glaciers. The
158 orthoimages revealed details in surface morphology that are typical for surging glaciers but barely visible for the
159 largest glaciers at the 30 or 15 m resolution of Landsat images. We also used Hexagon KH-9 scenes from July
160 1975 and June 1980 to generate orthoimages following Pieczonka et al. (2013). The scenes depict the regions
161 west of lake Karakul with a resolution of up to 6 m.

3.1.3 Google Earth and Bing Maps

163 The very high-resolution (a few m or better) satellite images available in Google Earth (GE) have been widely
164 used for numerous geoscientific applications (Liang et al., 2018). We used them here together with the satellite
165 images available on Bing Maps to confirm identified surging glaciers in the Landsat period, i.e. for visual checks
166 only. Sometimes the available time series in GE also allowed a proper identification of glacier surges when the
167 quiescent and/or active phases are captured (see examples in Lv et al., 2019). Interestingly, the images used in
168 Bing Maps were often complimentary to GE, i.e. provided excellent coverage when nothing useful was available
169 in GE and vice versa.

170

171 In Fig. 2 we provide a visual comparison of image sources displaying three surging glaciers in the central Pamir
172 to illustrate the visibility of details. We include examples from Corona, Hexagon, Landsat OLI as well as GeoEye
173 (from Bing Maps). The high-resolution images from Corona and Bing Maps clearly show the highly crevassed
174 surfaces (mainly for the two larger glaciers) that are not visible in the Landsat image. In the Landsat image, the
175 glacier boundary and debris-covered parts can be identified, but it is almost impossible to reveal the terminus of
176 Walter 731 (19) and Soldatov (20) glaciers in the static image. This is different when using animations that reveal
177 glacier termini clearly when they change position (Paul, 2015).

178

179 *Figure 2*

180

3.2 Digital elevation models (DEMs)

182 Several DEMs are freely available for the study region. This includes the Shuttle Radar Topography Mission
183 (SRTM) DEM (Rabus et al., 2003), the Advanced Spaceborne Thermal Emission and Reflection Radiometer
184 (ASTER) GDEMv3 (NASA, 2018), the ALOS PRISM DEM AW3D30 (Takaku et al., 2014), the High Mountain

Asia (HMA) DEM (Shean, 2017) and the DEM from the TanDEM-X mission (TDX) provided by DLR (German Aerospace Centre) (Wessel, 2016). They have different characteristics (sensor types, spatial resolution, artefacts, data voids, acquisition dates) and – apart from the HMA DEM – are used here for several purposes such as calculation of topographic characteristics and surface elevation changes (Table 2). A direct comparison of the DEMs using hillshades and DEM differences revealed that only the GDEMv3 and the AW3D30 DEM are free of data voids but that the AW3D30 has ~~partly~~ artefacts over glacier surfaces and too high elevations. We thus used the GDEMv3 to determine topographic characteristics for all glaciers.

Besides the orthoimages, we created DEMs from the 1968 Corona stereo pairs (cf. Goerlich et al., 2017) and used DEMs from 1975 Hexagon data (cf. Pieczonka et al., 2013). The AW3D30 DEM served as a height reference (Ground Control Points, Disparity Predictions) for the Corona DEM processing and the SRTM DEM for Hexagon. The main difference of the final DEMs is the coverage, where Corona covers only a small area (~15 km x 180 km) per stereo image pair compared to Hexagon (~130 km x 130 km). This results in a far larger effort to generate DEMs and orthophotos from Corona for a larger region.

We have used the ~~temporarily~~ better constrained DEMs from Corona (1968), SRTM (2000), AW3D30 (2006-2011), and TDX (2011-2014) to determine elevation changes over the periods of 1968 to 2000, 2000 to ~2009, and ~2009 to ~2012/14. Elevation differences were interpreted in a qualitative sense only as the typical pattern of elevation changes for surging glaciers (strong elevation gain in the lower and loss in the upper region during the active phase of a surge, and vice versa for the quiescent phase) can be clearly identified in most cases, i.e. changes are often much higher (100+ m) than the combined uncertainties of the two DEMs (e.g. Gardelle et al. 2013).

Table 2

3.3 Glacier outline datasets

We used the Karakoram / Pamir glacier inventory (GI-1) created by Mölg et al. (2018) as a basis for glacier identification and extent modification. This inventory provides a consistent dataset of manually corrected glacier outlines based on Landsat scenes acquired between 1998 and 2002 for the entire Pamir, including the ranges Kingtau, Ulugarttag and Muztagh in the Chinese part (see Fig. 1). As the inventory is a temporal snap shot and surge-type glaciers are in various stages of their surge cycle, they can be connected to a larger main glacier and thus not be analysed separately. To overcome this restriction, we have separated all part-time tributaries exhibiting their own dynamics from the glaciers they connect with and added the required new ice divides in the accumulation regions. This revised inventory (GI-2) is used as the base for all subsequent geomorphometric calculations. The separation follows the natural flow and extent of the larger glacier and required several iterations of adjustments, as the surge characteristics were often not clear from the beginning. After all surges have been identified, a sub-sample of GI-2 was created that only includes the glaciers that surged (inventory GI-3). The GI-3 sub-sample served as a base to digitise minimum and maximum glacier extents for all glaciers

223 exhibiting a visible change in terminus position. These datasets are saved in two additional inventories (GI-3min
224 and GI-3max, respectively).

4. Methods

4.1 Surge identification

227 Glacier surges can occur in very different forms with a likely continuous transition to unstable flow and regular
228 glacier advances. Hence, a clear identification of surge-type glaciers is not trivial even in their active phase and a
229 wide range of identification criteria has been suggested to distinguish them from all other glaciers (e.g. Sevestre
230 et al., 2015; Bhambri et al., 2017; Mukherjee et al., 2017). In this study, we focus on glaciers that had an active
231 surge phase during the investigated period 1988-2018, i.e. indirect evidences alone such as distorted or looped
232 moraines are not considered. Consequently, our sample is smaller than the one presented in the 'catalogue' by
233 Osipova et al. (1998), who listed 845 surge-type glaciers for the Pamir (i.e. 35% of the global sample by Sevestre
234 and Benn (2015)) in six distinct classes. Their inventory is also digitally available in the RGI using the simplified
235 classification scheme by Sevestre and Benn (2015), with the classes (their Table 4): confirmed (Category 3),
236 probable (2) and possible (1). With our focus on observed surges (with few exceptions) our sample would be in
237 the 'confirmed' type of which Osipova et al. (1998) list 61 and Sevestre and Benn (2015) 90 glaciers.

239 To identify surging glaciers, we started with the 'confirmed' samples listed by Osipova et al. (1998, 2010),
240 Kotlyakov et al. (2008) and Lv et al. (2019). These studies included all mountain ranges where we searched for
241 surging glaciers except the Rushanskii and Muztagh ranges. Our identification consists of four steps:

243 (I) At first, we analysed animations from the Landsat quicklooks to validate the findings of the four studies. Each
244 frame set was animated with slightly different samples (varying selection of animated scenes within one frame
245 set) to facilitate visibility of glacier dynamics in each region similar to Paul (2015). The qualitative analysis
246 tracked surface feature displacements and was applied to the entire study region. Collectively, this step revealed
247 139 surging glaciers during the period 1988-2018 (including glaciers that have just started surging).
248 (II) In the next step, we analysed the elevation change patterns of the various DEM difference maps in a
249 qualitative way (Mukherjee et al., 2017). Glaciers showing the typical opposing pattern of surface elevation
250 change along the glacier flow (lowering and thickening) were digitally marked and added to the sample, yielding
251 35 further glaciers from the 1968 to 2000 and 2000 to c. 2009 elevation difference maps. For this analysis it does
252 not matter in which region of a glacier the pattern occurs (e.g. internal surges may appear higher up and do not
253 reach the terminus). Two examples of the related DEM difference maps are displayed in Fig. 3, revealing for
254 some glaciers the typical surge pattern. This method helped in detecting internal surges with limited or no
255 changes of the terminus position and/or where crevasses or shear margins are difficult to detect.

257 *Figure 3*

(III) In this step, we analysed individual image pairs in detail using flicker images, i.e. going back and forth between two images only (Kääb et al. 2003). For a clear before/after distinction, this analysis was restricted to the best scenes available for a specific region (e.g. without clouds, seasonal snow or deep shadows). We here also used the contrast-enhanced false colour infrared images from the MSS scenes, several 15 m panchromatic images of ETM+ and OLI and the declassified orthoimages. An additional 27 surging glaciers could be identified this way.

(IV) In the final step, we checked the identified glaciers with the partially very high-resolution images available in GE and Bing Maps to also analyse morphological characteristics of the glacier surfaces in detail, their shape and also possible changes in extent (Lv et al., 2019). Despite the variability in acquisition years, this allowed us to remove a few glaciers (7) from the sample (in most cases the 'surges' were likely just advances) and also adding 12 new ones. We decided for glacier advances when the glacier does not show any of the typical surface features such as a heavily crevassed surface, shear margins or collapsing/down-wasting patterns at the tongue and a comparably small and/or slow advance. At this stage, we started introducing indirect evidence (surface features) to the classification and thus checked back if the (mostly small) glaciers have really surged using animations. In some cases it was necessary to interpret results from steps (I) to (III) collectively for a reasonable result.

Based on the created inventory subset with surging glaciers only (GI-3), we digitised the minimum (GI-3min) and maximum (GI-3max) extent of all glaciers based on the satellite images described in Section 3.1. For glaciers with more than one surge, the respectively largest and smallest extents were digitised (Fig. 4). Whereas maximum extents are in most cases well identifiable, outlines for GI-3min can have larger uncertainties due to the difficulties in clearly identifying the new terminus among the often debris-covered and down-wasting ice from the previous surge. Ideally, the minimum extent is identified once the next surge has started, but for many glaciers this did not happen during the observation period.

Figure 4

4.2 Surge characteristics and classification

There are a wide range of possibilities to characterise surges as they have a high variability of appearance and dynamics (e.g. Bhambri et al. 2017). For the GI-3min inventory we have determined a series of key surge characteristics in the attribute table (e.g. surge start / end / duration, and distance) and a simplified classification according to a pre-defined criteria set for statistical analysis and comparison with other regions. It has to be noted that a precise start/end year was often difficult to determine either due to missing satellite data, but also when surge initiation is related to a mass wave coming down from higher elevations (taking a few years) or when remaining dead ice from a previous surge was reactivated. We here defined the start of a surge as the year when an advance of the terminus or a mass wave higher up the glacier (as not all surges show a terminus advance) is detectable. The end of the active phase (maximum extent) is reached when all surge dynamics settle and the

296 quiescent phase begins. The surge duration is calculated by subtracting the start year from the end year of the

297 surge. The latter was easier to determine than minimum extents in most cases.

298

299 To illustrate a few of the possible surge types and interactions, Fig. 5 displays a sketch map of three glaciers that

300 are all surging at some stage. Starting with a surge of the permanently connected tributary (2) in Fig. 5a, this

301 surge is at its maximum extent in Fig. 5b and the ice from the surge is already slightly moved downstream by the

302 flow of the main glacier (1). In addition, glacier (3) started surging in the meantime, connects to the main glacier

303 in Fig. 5b and enters glacier (1) in Fig. 5c where it also reaches its maximum extent. Some time later (Fig. 5d),

304 also the main glacier (1) is in full surge mode and transports the surge marks of both tributary surges

305 downstream, stretching and possibly deforming them. This illustrates the variety of surge interactions (by far not

306 all) and the difficulty to define maximum extents of tributary glaciers. Their surge marks are moved downstream

307 by the main glacier during or near the end of their own surge due to its normal flow or a surge of the main

308 glacier. Accordingly, there is also some uncertainty in the timing of the surge end for glaciers (2) and (3). In this

309 case the main glacier body (1) would have listed two surges in the attribute table of GI-3min and would have

310 been selected to receive the surging classification code.

311

312 *Figure 5*

313

314 For the classification scheme, we used the following criteria and values for each glacier:

315 (A) 'surging?': no 0, yes 1, if yes:

316 (B) glacier tongue: free end 1, connects to another glacier 2, tributary 3

317 (C) type of surge: advancing 1, internal 2, combined 3

318 (D) active phase duration: 1-3 years 1, 4-10 years 2, >10 years 3

319 (E) terminus advance: none 0, short (<1 km) 1, medium (1-2.5 km) 2, long (> 2.5 km) 3.

320 In (C), the 'advancing' type defines a glacier that has a visible terminus change, 'internal' has no advance but

321 either a visible mass wave in the Landsat images or in the DEM difference images. The combined type describes

322 glaciers that show a mass wave within the glacier reaching the terminus and pushing it further down.

323 Hence, the entry in the attribute table of GI-2 is either 0 or 1 and stored in a separate 'surge' column. The

324 resulting code from our classification in GI-3min is then for example 2123. This means that the glacier is

325 connected to another glacier during its surge, that it has an advancing tongue and surged over a period of 4-10

326 years over a long distance. In the case the glacier already surged in 1988 or was still surging in 2018, these two

327 years were used as the start or end date. Such dates indicate that the real surge duration is likely longer than given

328 in the table.

329 **4.3 Topographic and other information**

330 For all glaciers in GI-2, we calculated the following attributes according to Paul et al. (2002, 2009): centre point

331 latitude and longitude, area in km^2, minimum, maximum, mean, and median elevation, mean slope and aspect,

332 and aspect sector. Mean values are calculated as the arithmetic average of all DEM cells covered by the

333 respective glacier. All attributes are also transferred to GI-3, and additionally calculated for GI-3min and GI-

334 3max. The attributes of GI-2/GI-3 depict the glacier state around the year 2000. For GI-3min/GI-3max

335 attribute date varies between 1988 and 2018 due to the minimum and maximum extent of the glaciers. All

336 elevation dependent attributes are based on ASTER GDEMv3 elevations.

5. Results

5.1 Distribution and topographic characteristics of surge and other glaciers

339 From the ~13500 glaciers in the study region, 186 have been identified as surging glaciers of which 206 spatially

340 distinct surges have been identified between 1988 and 2018. Their occurrence is clustered in the central, northern

341 (central and western Pamir Alai, Fedchenko and 'Petr Alervogo East') and eastern ranges (Muztagh and

342 Ulugarttag) (Fig. 6). This pattern leaves a large gap for glacier surges around Lake Karakul and to the south of

343 the study region with few exceptions. Overall, the latter regions are dominated by comparably smaller glaciers

344 and drier climate, indicating that there might be a size and climatic threshold for surge activity as suggested by

345 Sevestre and Benn (2015).

346

347 *Figure 6*

348

349 The 186 surging glaciers cover a total area of ~2670 km^2 (with ~110 km² variability due to the surges). Eight of

350 them (~5%) are smaller than 1 km^2 covering an area of ~7 km^2, whereas 38% are larger than 10 km^2 covering an

351 area of 2170 km^2 (or 81%) (Table 3). Garmo Glacier main trunk (80) is the largest surging glacier (83 km^2) and

352 the largest non-surging glacier is Fedchenko. It is a huge dendritic valley glacier with a size of ~580 km^2 (without

353 the surging Bivachny tributary) and is covering 6% of the total glacier area. The region is thus dominated by the

354 vast size of Fedchenko Glacier with impacts on size-related distributions.

355

356 *Table 3*

357 The created inventories have a different count of entries due to different glacier states and topologic relations.

358 The generalised statistics for the sample with observed surges refer to the GI-3 inventory with 186 entries whilst

359 statistics for GI-3min and GI-3max have different numbers. Compared to the full sample of glaciers in GI-2

360 (13495), surging glaciers constitute 77% by number and 80% by area in the area class 50-100 km^2 (Fig. 7). They

361 are also dominating the size classes 10-50 and 100-500 km^2 (51% and 63% by area, respectively). When

362 considering all three size classes from 10 to 500 km^2, two thirds of the glaciers have surged in the observation

363 period, i.e. they are the rule rather than the exception. The 22 largest surging glaciers cover almost the same area

364 (1338 km^2) than the 163 smaller ones (1332 km^2).

365

366 *Figure 7*

367

368 The frequency distribution of aspect sectors of surging glaciers is only slightly different from all other glaciers

369 (Fig. 8a). Surging glaciers exposed to SW contribute almost 10% to the sample whereas only 3% of the other

370 glaciers are facing in this direction. The same applies to the area covered (Fig. 8b), where surging glaciers

cumulate ~370 km² and thus ¼ more area than the other glaciers (~300 km²) in this sector. On the other hand, the latter have higher percentages facing N and NE. The strong difference towards the N is mainly driven by Fedchenko Glacier.

Figure 8

The scatter plot showing median elevation vs. mean aspect (Fig. 9) reveals that mean elevations cover a wide range of values (from about 3500 to 6000 m) and that there is some dependence on aspect, i.e. glaciers facing south have a few hundred metres higher mean elevations. The surging glaciers largely follow the distribution, but have somewhat higher elevations in the southern and lower values in the northern aspect ranges compared to the other glaciers when considering mean values per sector. On average, the median elevation of surging glaciers is 4800 m a.s.l.

Figure 9

Median glacier elevations increase from west to east and show a small decrease in the most eastern and northern ranges (Pamir Alai) towards the outer glaciers (Fig. 10). The marked surging glaciers are mostly found along the outer boundary of the study region with generally lower median elevations. The near absence of surging glaciers in the inner Pamir with its generally higher median elevations is noteworthy. However, in the Mustagh region, glaciers with observed surges have the highest (5646 m) and surging glaciers in the 'Petr Alervogo west' region the lowest values (3429 m).

Figure 10

As surging glaciers have a bias towards larger sizes compared to all other glaciers (see Fig. 7), they also have slightly higher elevation ranges (Fig. 11a) and form the upper end of the sample. However, the spread of values for glaciers with a size of about 50 km^2 is very large, ranging from about 2000 to nearly 5000 m. The area-elevation distribution in Fig. 11b displays a smaller amount of area around the mean elevation compared to all other glaciers, which is likely due to the many small glaciers in these altitudes (see black circles in Fig. 10).

Figure 11

5.2 Observed changes

For a sample of 169 and 160 glaciers, we could map their minimum and maximum extent, respectively and for 148 surges we determined the surge duration which is completely within the observation period. For 15 glaciers, we observed a full surge cycle with the onset of the next surge and for six glaciers (Bivachny 63, Dzerzhinsky 104, Medvezhy 29, Right Dustiroz 31, Yazgulemdara 35, OID 1) two or more surges were observed over the study period. Both, the timing of the surges and their durations are highly variable (Fig. 12). Moreover, one has

409   to consider that several glaciers (>30) were already surging on the first available Landsat TM images (in 1988)

410   and several (>20) are still surging in 2017/2018. For both cases the surge duration could not be fully determined

411   and is thus longer than the values presented here.

412

413   *Figure 12*

414

415   The two histograms in Fig. 13 display a counting of the surges that started in a particular period (Fig. 13a) and of

416   the surge durations in 4-year bins (Fig. 13b). For both graphs it has to be considered that the first period

417   (1988/89) is including all glaciers that are already surging at that time. This gives a much higher number of

418   surges (66) compared to those that have only started in 1989 (27). For the surge duration counting in Fig. 13b this

419   means that shorter surge periods are over-represented and are indeed longer. Furthermore, the last period is not

420   complete (i.e. surges are on-going), which has the same effect on the counting. This results in possibly too high

421   and too low values in the first and last period, respectively. To circumvent this bias, we have also counted all

422   surges that took fully place within the period, i.e. started after 1989 and ended before 2017 (black bars in Fig.

423   13b). This sample is now smaller, but has still a reasonable ~~amount~~ of glaciers in all classes. Figure 13a reveals

424   that the number of surges that have started in the second and third period is the same and slowly declining

425   afterwards. The surge duration counting displayed in Fig. 13b has a peak at 1-5 years and very similar numbers

426   for the next four intervals. Only few glaciers (9) have surge durations exceeding 21 years. The combination start

427   year and duration gives the number of glaciers that are surging in a particular year. We found a steady increase in

428   this number from 1990 (54) to 2000 (114), with a plateau until 2008 (112) and a steady decrease afterwards (to

429   72 in 2018). In other words, in any year during the observation period at least 54 glaciers were actively surging in

430   the study region, up to a maximum of 129 glaciers in 2006. This is far more than expected.

431

432   *Figure 13*

433

434   The simplified typology (see Section 4.2) counting presented in Table 4 reveals that 75% of all glaciers have

435   freely advancing tongues, whereas 18% connect to another glacier at least in their maximum extent. From the

436   total sample of identified surging glaciers, 85% (176 glaciers) are considerably advancing whereas the remaining

437   15% (26) are surging internally with none or only a minor terminus advance. The latter were sometimes hard to

438   detect and required application of additional measures (see Section 3). From the glaciers with a substantial

439   terminus advance, most (49%) advance up to 1 km. Larger advances of up to 2.5 km are found for 27% of the

440   glaciers and 8.5% advanced more than 2.5 km (up to 6.7 km). Most of the surges with a change in terminus

441   position are situated in the central mountain ranges around Fedchenko Glacier, whereas the eastern ranges are

442   dominated by stable glaciers and internal surges (but with a high variability). The strongest advance has Oshanina

443   Glacier (9) in the Petr Alervogo East mountain range with 4078 m. For this analysis, we excluded all glacier

444   surges that were not fully covered by the observation period (start before 1988, end after 2018.

445

446   *Table 4*

447

448 One of the most active glaciers is Medvezhy Glacier (29) with a surge cycle of only ~10 years and an active
449 period of just 2 years (Kotlyakov et al., 2018). Further glaciers with relatively short (≤ 5 years) active phases are
450 spread all over the study region. During the active surge phase, 128 glaciers increased their area by a total of
451 ~119 km², which is 6% of their total area (GI-3min) and 4% of the total area in the GI-2 inventory. On average,
452 the minimum elevation decreased from 3954 m a.s.l. to 3793 m a.s.l., but individual glaciers are reaching to more
453 than 800 m lower elevations at their maximum extent. The change in minimum elevation due to a surge does not
454 depend on the elevation range (or size) of the glacier. This is also related to the fact that several large glaciers
455 show mostly internal surges with maybe only a small advance of the tongue. Similarly, ~~also~~ length changes due
456 to a surge do not depend on glacier size or length. However, it is noteworthy that some glaciers change their
457 length by about a factor of almost two (41).

6. Discussion

6.1 Characteristics of the surging glaciers and their surges

460 Surging glaciers dominate the area classes above 10 km², which would confirm earlier observations that surging
461 glaciers are comparably large (Barrand and Murray, 2006; Clarke et al., 1986; Mukherjee et al., 2017). However,
462 we found that they can also be smaller than 1 km², down to 0.3 km². Why such small glaciers surge, often
463 increasing their length considerably, needs to be further investigated. We also have to mention that there might be
464 even smaller glaciers that were not detected due to the coarse resolution of the satellite data, i.e. our sample is
465 somewhat biased towards larger glaciers. Whereas the aspect distribution of surging glaciers is very similar to all
466 other glaciers (Fig. 8), they seem to have lower median elevations than other glaciers when facing north and
467 higher ones when facing south (Fig. 9). We do not have a physical explanation for this and assume it might only
468 be an artefact of the sampling. Their spatial distribution, on the other hand, is more peculiar as they are mostly
469 found in the outer regions of the study site (Figs. 5 and 10). Their higher share of large elevation ranges (Fig.
470 11a) is related to their generally larger size and their hypsometry is very similar to other glaciers.
471
472 Within the period considered here, the starting dates of surges are comparably random (Fig. 12), indicating a
473 limited impact of climatic trends on the timing. The high number of surging glaciers (about 55 to max 120) in any
474 year is remarkable and can only be found in the Karakoram (Bhambri et al., 2017). Whether the constant increase
475 (decline) before the year 2000 ~~(after 2008)~~ is an artefact of the sampling or has other reasons needs to be
476 investigated in a further study. Surge durations (11 years in the mean) are as diverse as in the Karakoram
477 (Bhambri et al., 2017; Paul, 2020). However, complete surge cycles are not observed for many glaciers (from one
478 start of an active phase to the next), so this impression is biased by the observation window. Due to gaps in
479 satellite data availability, we might have missed a few glaciers displaying only (short) internal surges, so the real
480 number of surging glaciers might be even higher and the number of glaciers with a short duration of active phases
481 higher than in our sample.

6.2 Criteria to identify surges

The criteria we applied to identify surges were handled ~~flexible~~ to consider the wide range of surge types found in the region. However, the differentiation between surging and 'only' advancing glaciers is sometimes challenging and other interpretations are possible. The very high-resolution images ~~as~~ available for our study site from Corona / Hexagon and Google Earth / Bing Maps did not help much in determining the timing of a surge (due to the large temporal gaps), but were most helpful in confirming the surge nature of a glacier in previous and recent times, respectively (Lv et al. 2019, Paul 2020). The historic images clearly reveal that many glaciers in the Pamir Mountains have also surged in the 1970s, however we have not used them here to derive the timing of these earlier surges as this would be a large additional exercise and the temporal density of available images might not be sufficient. However, we used them to confirm additional minimum and maximum extents.

6.3 Uncertainties

Regarding the uncertainties of the derived topographic characteristics, one has to consider that we used the GI-1 basis inventory from around 2000 with a DEM (GDEMv3) from around 2008 (NASA, 2018). The DEM has local artefacts, is void filled and the timing of both datasets does not match. The latter is in particular the case for glaciers that surged between 2000 and 2009 and had strong changes in geometry. The strongest impact is likely on minimum elevation, but also median elevation, aspect and mean slope might be impacted. There is little we can do about this uncertainty, as otherwise we would need a DEM from nearly every year, synchronous with the timing of the minimum glacier extent. However, for the overall statistical analysis of the datasets presented here, the impact of the temporal mismatch on the graphs is likely small. Of course, when individual glaciers are analysed, this mismatch has to be considered (Frey and Paul, 2012).

Regarding the timing of the observed surges, we face the following uncertainties:

a) We have only analysed the time window 1988 to 2018; the assigned duration of surges starting before 1988 or ending after 2018 is thus too short,

b) we only include glaciers with an active surge phase between 1988 and 2018; the real number of glaciers in the study region that surged in the past might thus be higher,

c) for most regions we do not have usable satellite images in every year (e.g. due to snow and clouds); this adds to the uncertainty of the start/end assignment and could even result in completely missed short-lived internal surges,

d) the spatial resolution of Landsat sometimes impacts a proper identification of the terminus, in particular when debris-covered; this leads to uncertainties in the timing,

e) due to residual dead ice in the glacier forefield and debris cover, the timing of the minimum extent is more difficult to define than the maximum; in uncertain cases we used the extent from GI-3, and

f) when surges start with a mass wave and/or stay internal (no terminus advance), the timing derived from visual analysis will likely be different from studies analysing flow velocities.

Collectively, it is likely that other analysts derive different start/end dates of individual surges, but in most cases the difference will not exceed a few years. This will thus not affect the overall conclusions about the highly variable timing of surges and surge durations.

The ~~here presented~~ assignment of surge classes should be robust as we used qualitative and categorised criteria that will not change much for a different interpretation. However, not all surges of the same glacier end up in the same class. For example, if a recent surge is more dynamic than a previous one, it might reach another glacier and become a part-time tributary. Also internal surges might have shown advancing termini before and are thus not strictly internal. Hence, the assigned classes can vary for other surges. In general, we only assigned the characteristics of the surge of the main glacier trunk to the attribute table.

6.4 Comparison to other inventories

Compared to previous studies, we identified several new surging glaciers. Some of the probable or possible (category 2 and 3) surges listed in Osipova et al. (1998) have indeed surged and are now included in our inventory. Most others found in these categories could not be confirmed as the morphological details used to identify surge activities are only visible in very high-resolution imagery (at least 2 m) rather than with 30 or 15 m Landsat data we used here. It is, however, well possible that they surged outside our observation window.

Sevestre and Benn (2015) presented 820 possible surge-type glaciers in the Pamir mainly based on the inventory by Osipova et al. (1998). Our findings are in good agreement with the 51 most reliably classified (category 3) surge-type glaciers marked in the RGI (we include 45 of them). Our 132 additional surging glaciers belong mostly (55 of 188) to category (2) in the RGI, and a few (18 of 322) belong to category (1). The remaining 52 surging glaciers were not indicated as surge-type in the RGI. When considering the 14 further glaciers which were mentioned by Lv et al. (2019), 38 (20.5% of the total sample) so far unknown surging glaciers have been identified here for the Pamir. Outlines from two of our surging glaciers (65 and 64) are missing in the RGI 6.0.

Compared to Lv et al. (2019), we identified three further surging glaciers (16 in total) in the King Tau and Ulugarttag sub-regions. Apart from surge-type glaciers, their study also classified four glaciers as advancing, eleven as stable and one retreating. We classified one of their advancing and three of their stable glaciers as surging. This new interpretation results from our longer observation period and the DEM difference images revealing the typical mass redistribution patterns. The surging glaciers described by Kotlyakov et al. (2008) are in full agreement with our findings. The above-mentioned numbers have to be interpreted with some care, as we compared two different inventories with individual glacier divides. Thus, a direct and one-to-one comparison is challenging.

7. Conclusions

In this study, we presented a new inventory of surging glaciers for the Pamir Mountains. The analysis is based on results from earlier studies, Landsat imagery acquired over the period 1988 to 2018, the SRTM, ASTER GDEMv3 and ALOS DEM and declassified very-high resolution images from Corona and Hexagon. Using animations and flicker images for the Landsat time series in combination with the elevation change patterns from DEM differencing, we detected 206 spatially distinct glacier surges within 186 glacier bodies. The new dataset is

556 in good agreement with previous compilations of surging glaciers and confirmed surges for 133 new glaciers that
557 were so far only marked as surge-type probable or possible. We further digitized minimum and maximum extent
558 of 169 and 160 glaciers, respectively, and determined the timing for about ¾ of all surges. The temporal
559 distribution is random concerning timing and surge duration (mean value 11 years), but the high number of active
560 surges in any year (between 54 and 120) was unexpected and ~~in this amount only known from~~ the Karakoram.
561 The distribution of surging glaciers is biased towards the central, northern and eastern mountain ranges. Their
562 sizes range from 0.3 to 143 km² and they are dominating the size-class distribution above 10 km². Three glaciers
563 descend by more than 800 m and five increased their length by a factor of more than 2 during a surge. However,
564 advance distances are not related to original glacier length as several large glaciers only show internal surges or
565 very small advances. The three inventories created in this study (GI-3, GI-3min, GI-3max) are available in the
566 Supplemental Material to serve as a base for further investigations.

8. Data availability

568 The dataset can be downloaded from: https://doi.pangaea.de/10.1594/PANGAEA.914150 (Goerlich et al., 2020).

Author contribution

570 F.G. and F.P. designed the study, analysed the datasets and wrote the manuscript, F.G. processed the data and
571 prepared all figures and datasets. T.B. provided additional literature and datasets. All authors contributed to the
572 writing and editing of the manuscript.

Competing interests

574 The authors declare that they have no conflict of interest.

Acknowledgements

576 The work of F.G. and F.P. was supported by the ESA projects Glaciers_cci (4000109873/14/I-NB) and
577 Glaciers_cci+ (4000127593/19/I-NB), the work of T.B. was partially supported by the Strategic Priority Research
578 Program of Chinese Academy of Sciences (XDA20100300). The AW3D30 DEM is provided by the Japan
579 Aerospace Exploration Agency (http://www.eorc.jaxa.jp/ALOS/en/aw3d30/index.htm) ©JAXA. All Corona,
580 Hexagon and Landsat images used in this study were provided by USGS and downloaded from
581 earthexplorer.usgs.gov. We thank P. Rastner for supporting us in calculating the topographic parameters for
582 several states of the inventory, K. Mukherjee for providing the Hexagon DEMs from 1975 and H. Machguth for
583 providing the centre lines for determination of glacier length and length changes. We thank the two anonymous
584 reviewers for their conscientious work to improve this study.

References

Barrand, N. E. and Murray, T.: Multivariate Controls on the Incidence of Glacier Surging in the Karakoram Himalaya, Arctic, Antarct. Alp. Res., 38(4), 489–498, doi:10.1657/1523-0430(2006)38[489:MCOTIO]2.0.CO;2, 2006.

Berthier, E. and Brun, F.: Karakoram geodetic glacier mass balances between 2008 and 2016: Persistence of the anomaly and influence of a large rock avalanche on Siachen Glacier, J. Glaciol., 65(251), 494–507, doi:10.1017/jog.2019.32, 2019.

Bhambri, R., Hewitt, K., Kawishwar, P. and Pratap, B.: Surge-type and surge-modified glaciers in the Karakoram, Sci. Rep., 7(15391), 1–14, doi:10.1038/s41598-017-15473-8, 2017.

Bolch, T., Pieczonka, T., Mukherjee, K. and Shea, J.: Brief communication: Glaciers in the Hunza catchment (Karakoram) have been nearly in balance since the 1970s, Cryosphere, 11(1), 531–539, doi:10.5194/tc-11-531-2017, 2017.

Brun, F., Berthier, E., Wagnon, P., Kääb, A. and Treichler, D.: A spatially resolved estimate of High Mountain Asia glacier mass balances from 2000 to 2016, Nat. Geosci., 10(9), 668–673, doi:10.1038/ngeo2999, 2017.

Clarke, K. C., Sciimoi, P., Simon, C. and Ommanney, L.: Characteristics of Surge-Type Glaciers, J. Geophys. Res., 91(5), 7165–7180, doi:10.1029/JB091iB07p07165, 1986.

Dolgushin, L. D. and Osipova, G. B.: New Data on the recent Glacier Surges, Mater. Glyatsiol., 18, 191–217, 1971.

Dolgushin, L. D. and Osipova, G. B.: Glacier surges and the problem of their forecasting, IAHS Publ, (104), 292–304, 1975.

Dowdeswell, J. A., Gorman, M. R., Macheret, Y. Y., Moskalevsky, M. Y. and Hagen, J. O.: Digital comparison of high resolution Sojuzkarta KFA-1000 imagery of ice masses with Landsat and SPOT data, Ann. Glaciol., 17, 105–112, doi:10.3189/S0260305500012684, 1993.

Dowdeswell, J. A., Glazovsky, A. F. and Macheret, Y. Y.: Ice divides and drainage basins on the ice caps of Franz Josef Land, Russian High Arctic, defined from Landsat, KFA-1000, and ERS-1 SAR satellite imagery, Artic Alp. Res., 27(3), 264–270, doi:10.1080/00040851.1995.12003121, 1995.

Falaschi, D., Bolch, T., Lenzano, M. G., Tadono, T., Lo Vecchio, A. and Lenzano, L.: New evidence of glacier surges in the Central Andes of Argentina and Chile, Prog. Phys. Geogr., 42(6), 792–825, doi:10.1177/0309133318803014, 2018.

Finaev, A. F., Shiyin, L., Weijia, B. and Li, J.: Climate Change And Water Potential Of The Pamir Mountains, Geogr. Environ. Sustain., 9(3), 88–105, doi:10.15356/2071-9388_03v09_2016_06, 2016.

Frey, H. and Paul, F.: On the suitability of the SRTM DEM and ASTER GDEM for the compilation of: Topographic parameters in glacier inventories, Int. J. Appl. Earth Obs. Geoinf., 18(1), 480–490, doi:10.1016/j.jag.2011.09.020, 2012.

Galiatsatos, N.: The Shift from Film to Digital Product: Focus on CORONA Imagery, Photogramm. - Fernerkundung - Geoinf., 2009(3), 251–260, doi:10.1127/0935-1221/2009/0020, 2009.

Gardelle, J., Berthier, E., Arnaud, Y. and Kääb, A.: Region-wide glacier mass balances over the Pamir-Karakoram-Himalaya during 1999-2011, Cryosphere, 7(4), 1263–1286, doi:10.5194/tc-7-1263-2013, 2013.

Goerlich, F., Bolch, T., Mukherjee, K. and Pieczonka, T.: Glacier Mass Loss during the 1960s and 1970s in the Ak-Shirak Range (Kyrgyzstan) from Multiple Stereoscopic Corona and Hexagon Imagery, Remote Sens., 9(275), doi:10.3390/rs9030275, 2017.

Goerlich, F., Bolch, T., Paul, F.: Inventory of surging glaciers in the Pamir. PANGAEA, https://doi.pangaea.de/10.1594/PANGAEA.914150, 2020.

Herreid, S. and Truffer, M.: Journal of Geophysical Research : Earth Surface Automated detection of unstable glacier flow and a spectrum of speedup behavior in the Alaska Range Special Section :, J. Geophys. Res. Earth Surf., 121(1), 64–81, doi:10.1002/2015JF003502.Surge-type, 2016.

Holzer, N., Golletz, T., Buchroithner, M. F. and Bolch, T.: Glacier Variations in the Trans Alai Massif and the Lake Karakul Catchment (Northeastern Pamir) Measured from Space, in R.P. Singh, U. Schikhoff, & S. Mal (Eds.): Climate Change, Glacier Response, and Vegetation Dynamics in the Himalaya, edited by R. P. Singh, U. Schikhoff, and S. Mal, pp. 139–153, Springer, Cham., 2016.

Kääb, A., Isakowski, Y., Paul, F., Neumann, A. and Winter, R.: Glaziale und periglaziale Prozesse: Von der statischen zur dynamischen Visualisierung, Kartographische Nachrichten, 53(5), 206–212, 2003.

Kotlyakov, V. M., Desinov, L. V., Osipova, G. B., Hauser, M., Tsvetkov, D. G. and Schneider, J. F.: Events in 2002 on Russian Geographical Society (RGO) Glacier, Pamirs, Mater. Glyatsiol., 95, 221–230, 2003.

Kotlyakov, V. M., Osipova, G. B. and Tsvetkov, D. G.: Monitoring of the Pamirs surging glaciers from space, Ann. Glaciol., 48, 125–134, doi:10.3189/172756408784700608, 2008.

Kotlyakov, V. M., Chernova, L. P., Khromova, T. E., Muraviev, A. Y., Kachalin, A. B. and Tiuflin, A. S.:

Unique Surges of Medvezhy Glacier, Dokl. Earth Sci., 483(2), 1547–1552, doi:10.1134/s1028334x18120152, 2018.

Lambrecht, A., Mayer, C., Aizen, V., Floricioiu, D. and Surazakov, A.: The evolution of Fedchenko glacier in the Pamir, Tajikistan, during the past eight decades, J. Glaciol., 60(220), 233–244, doi:10.3189/2014JoG13J110, 2014.

Lambrecht, A., Mayer, C., Wendt, A., Floricioiu, D. and Völksen, C.: Elevation change of Fedchenko Glacier, Pamir Mountains, from GNSS field measurements and TanDEM-X elevation models, with a focus on the upper glacier, J. Glaciol., 64(246), 637–648, doi:10.1017/jog.2018.52, 2018.

Liang, L., Cuo, L. and Liu, Q.: The energy and mass balance of a continental glacier: Dongkemadi Glacier in central Tibetan Plateau, Sci. Rep., 8(1), 1–8, doi:10.1038/s41598-018-31228-5, 2018.

Lv, M., Guo, H., Lu, X., Liu, G., Yan, S., Ruan, Z., Ding, Y. and Quincey, D. J.: Characterizing the behaviour of surge- and non-surge-type glaciers in the Kingata Mountains, eastern Pamir, from 1999 to 2016, Cryosphere, 13(1), 219–236, doi:10.5194/tc-13-219-2019, 2019.

Machguth, H. and Huss, M.: The length of the world's glaciers a new approach for the global calculation of center lines, Cryosphere, 8(5), 1741–1755, doi:10.5194/tc-8-1741-2014, 2014.

Maussion, F., Scherer, D., Mölg, T., Collier, E., Curio, J. and Finkelnburg, R.: Precipitation seasonality and variability over the Tibetan Plateau as resolved by the high Asia reanalysis, J. Clim., 27(5), 1910–1927, doi:10.1175/JCLI-D-13-00282.1, 2014.

Minora, U., Bocchiola, D., D'Agata, C., Maragno, D., Mayer, C., Lambrecht, A., Vuillermoz, E., Senese, A., Compostella, C., Smiraglia, C. and Diolaiuti, G. A.: Glacier area stability in the Central Karakoram National Park (Pakistan) in 2001–2010: The "Karakoram Anomaly" in the spotlight., 2016.

Mölg, N., Bolch, T., Rastner, P., Strozzi, T. and Paul, F.: A consistent glacier inventory for Karakoram and Pamir derived from Landsat data: Distribution of debris cover and mapping challenges, Earth Syst. Sci. Data, 10(4), 1807–1827, doi:10.5194/essd-10-1807-2018, 2018.

Mukherjee, K., Bolch, T., Goerlich, F., Kutuzov, S., Osmonov, A., Pieczonka, T. and Shesterova, I.: Surge-type glaciers in the Tien Shan (Central Asia), Arctic, Antarct. Alp. Res., 49(1), 147–171, doi:10.1657/AAAR0016-021, 2017.

NASA/METI/AIST/Japan Spacesystems, and U.S./Japan ASTER Science Team: ASTER Global Digital Elevation Model V003, distributed by NASA EOSDIS Land Processes DAAC, https://doi.org/10.5067/ASTER/ASTGTM.003, 2018.

Osipova, G. B.: Fifty years of studying the Medvezhiy Glacier (West Pamirs) by the Institute of Geography, RAS, Ice Snow, 1, 129–140, doi:10.15356/2076-6734-2015-1-129-140, 2015. (in Russian)

Osipova, G. B. and Khromova, T. E.: Electonic data base "Surging glaciers of Pamir" Ice Snow, 50(4), 15–24, 2010. (in Russian)

Osipova, G. B., Tsvetkov, D. G., Schetinnikov, A. S. and Rudak, M. S.: Inventory of surging glaciers of the Pamirs, Mater. Glyatsiol., 85, 3–136, 1998. (in Russian)

Paul, F., Kääb, A., Maisch, M., Kellenberger, T. and Haeberli, W.: The new remote-sensing-derived Swiss glacier inventory: I. Methods, Ann. Glaciol., 34, 355–361, doi:10.3189/172756402781817473, 2002.

Paul, F., Barry, R. G., Cogley, J. G., Frey, H., Haeberli, W., Ohmura, A., Ommanney, C. S. L., Raup, B., Rivera, A. and Zemp, M.: Recommendations for the compilation of glacier inventory data from digital sources, Ann. Glaciol., 50(53), 119–126, doi:10.3189/172756410790595778, 2009.

Paul, F.: Revealing glacier flow and surge dynamics from animated satellite image sequences: Examples from the Karakoram, Cryosphere, 9(6), 2201–2214, doi:10.5194/tc-9-2201-2015, 2015.

Paul, F.: A 60-year chronology of glacier surges in the central Karakoram from the analysis of satellite image time-series, Geomorphology, 352, 106993, doi:10.1016/j.geomorph.2019.106993, 2020.

Pieczonka, T., Bolch, T. and Buchroithner, M.: Generation and evaluation of multitemporal digital terrain models of the Mt. Everest area from different optical sensors, ISPRS J. Photogramm. Remote Sens., 66(6), 927–940, doi:10.1016/j.isprsjprs.2011.07.003, 2011.

Pieczonka, T., Bolch, T., Junfeng, W. and Shiyin, L.: Heterogeneous mass loss of glaciers in the Aksu-Tarim Catchment (Central Tien Shan) revealed by 1976 KH-9 Hexagon and 2009 SPOT-5 stereo imagery, Remote Sens. Environ., 130, 233–244, doi:10.1016/j.rse.2012.11.020, 2013.

Quincey, D. J., Glasser, N. F., Cook, S. J. and Luckman, A.: Heterogeneity in Karakoram glacier surges, J. Geophys. Res. Earth Surf., 120(7), 1288–1300, doi:10.1002/2015JF003515, 2015.

Rabus, B., Eineder, M., Roth, A. and Bamler, R.: The shuttle radar topography mission—a new class of digital elevation models acquired by spaceborne radar, ISPRS J. Photogramm. Remote Sens., 57(4), 241–262, doi:10.1016/S0924-2716(02)00124-7, 2003.

Rankl, M. and Braun, M.: Glacier elevation and mass changes over the central Karakoram region estimated from TanDEM-X and SRTM/X-SAR digital elevation models, Ann. Glaciol., 57(71), 273–281, doi:10.3189/2016AoG71A024, 2016.

701 Round, V., Leinss, S., Huss, M., Haemmig, C. and Hajnsek, I.: Surge dynamics and lake outbursts of Kyagar
702   Glacier, Karakoram, Cryosphere, 11(2), 723–739, doi:10.5194/tc-11-723-2017, 2017.
703 Sevestre, H. and Benn, D. I.: Climatic and geometric controls on the global distribution of surge-type glaciers:
704   Implications for a unifying model of surging, J. Glaciol., 61(228), 646–662, doi:10.3189/2015JoG14J136,
705   2015.
706 Shean, D.: High Mountain Asia 8-meter DEM Mosaics Derived from Optical Imagery, Version, Boulder,
707   Colorado., 2017.
708 Steiner, J. F., Kraaijenbrink, P. D. A., Jiduc, S. G. and Immerzeel, W. W.: Brief Communication : The Khurdopin
709   glacier surge revisited – extreme flow velocities and formation of a dammed lake in 2017, Cryosph., 12(1),
710   95–101, 2018.
711 Tachikawa, T., Hato, M., Kaku, M. and Iwasaki, A.: Characteristics of ASTER GDEM version 2, Vancouver,
712   BC., 2011.
713 Takaku, J., Tadono, T. and Tsutsui, K.: Generation of high resolution global DSM from ALOS PRISM, Int. Arch.
714   Photogramm. Remote Sens. Spat. Inf. Sci. - ISPRS Arch., 40(4), 243–248, doi:10.5194/isprsarchives-XL-4-
715   243-2014, 2014.
716 Wendt, A., Mayer, C., Lambrecht, A. and Floricioiu, D.: A Glacier Surge of Bivachny Glacier, Pamir Mountains,
717   Observed by a Time Series of High-Resolution Digital Elevation Models and Glacier Velocities, Remote
718   Sens., 9(4), 388, doi:10.3390/rs9040388, 2017.
719 Wessel, B.: TanDEM-X Ground Segment – DEM Products Specification Document", Oberpfaffenhofen. [online]
720   Available from: https://tandemx-science.dlr.de/, 2016.
721 Yasuda, T. and Furuya, M.: Dynamics of surge-type glaciers in West Kunlun Shan, Northwestern Tibet, J.
722   Geophys. Res. F Earth Surf., 120(11), 2393–2405, doi:10.1002/2015JF003511, 2015.
723 Zhang, H., Zhang, F., Zhang, G., Ma, Y., Yang, K. and Ye, M.: Daily air temperature estimation on glacier
724   surfaces in the Tibetan Plateau using MODIS LST data, J. Glaciol., 64(243), 132–147,
725   doi:10.1017/jog.2018.6, 2018.
726

727 **Tables**

728

729 *Table 1: Main characteristics of the satellite scenes used (see Table S1 for scene list).*

Satellite	Sensor	Resolution	Period	Purpose
Corona	KH-4	2-5 m	1968	DEM generation, high-res. info
Hexagon	KH-9	5-10 m	1975/1980	Additional DEM and high-res. info
Landsat	MSS	60 m	1972-1980	Extension back in time
Landsat	TM	30 m	1989-2012	Animation
Landsat	ETM+	30 m	1999-2018	Animation
Landsat	OLI	30 m	2013-2018	Animation

730
731

732 *Table 2: Selected characteristics of available DEMs and their usage in this study.*

DEM	Type	Sensor	Resolution	Acquisition period	Date of tiles?	Usage
GDEMv3	optical	ASTER	30 m	2000-2013	No	Heights for Corona, topographic parameters
SRTM	SAR-C	SRTM	30 m	Feb 2000	Yes	Elevation changes
ALOS	optical	PRISM	30 m	2007-2011	No	elevation changes 2000 to 2009
TDX	SAR-X	TanDEM-X	90 m	2012-2015	No	Elevation changes ~2009 to ~2014
Corona	optical	KH4-B	15 m	1968	Yes	Elevation changes 1968 to 2000; Orthophoto

733

734 *Table 3: Size class distribution of surging glaciers and other glaciers of GI-2 and GI-3.*

Size Class km²		<0.05	0.05 – 0.1	0.1 – 0.5	0.5 – 1	1 – 5	5 – 10	10 – 50	50 – 100	100 – 500	>500
other glaciers	km²	103.7	154.7	1104	1090.7	3353.4	1172.7	1190.1	167.8	154	580.3
	%	1.1	1.7	12.2	12	37	12.9	13.1	1.9	1.7	6.4
surging glaciers	km²	0	0	0.4	6.1	174.2	319.7	1229	682.9	262.6	0
	%	0	0	0	0.2	6.5	12	46	25.5	9.8	0
all glaciers	km²	103.7	154.7	1104.5	1096.9	3527.6	1492.3	2419.2	850.6	416.6	580.3
	%	0.9	1.3	9.4	9.3	30	12.7	20.6	7.2	3.5	4.9
Surging proportion in %		0	0	0	0	0	21.4	50.8	80.3	63	0

735
736
737 *Table 4:* ==*Results of the surging classification*== *(counting per class). Glaciers with incomplete active surge phases*
738 *(starting before 1988 or ending after 2018 and marked with a "0" for the distance criterion) are not listed here.*

Criteria	1	2	3	Total
Tongue	150	32	16	198
Type	169	25	4	198
Duration	21	63	114	198
Distance	106	53	13	172

739

740

Figures
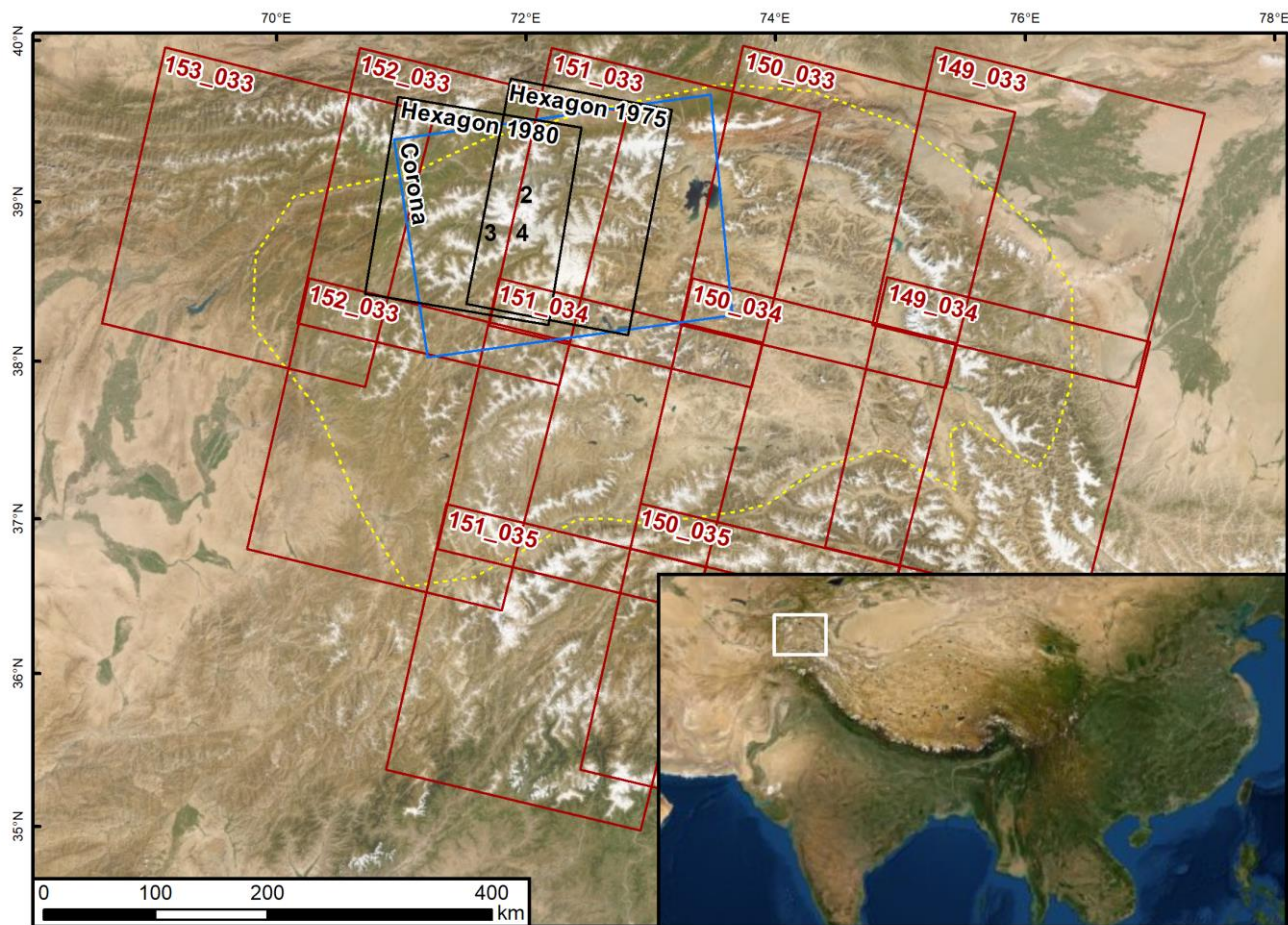
Fig. 1: Location of the study region (white square in the inset) and footprints of the Corona (blue), Hexagon (black) and Landsat (red) scenes used in this study. The dashed yellow line marks the perimeter of the study region. The location of the sub-regions displayed in Figs. 2, 3 and 4 are marked with their respective numbers. Image sources: screenshots from © Google Earth.
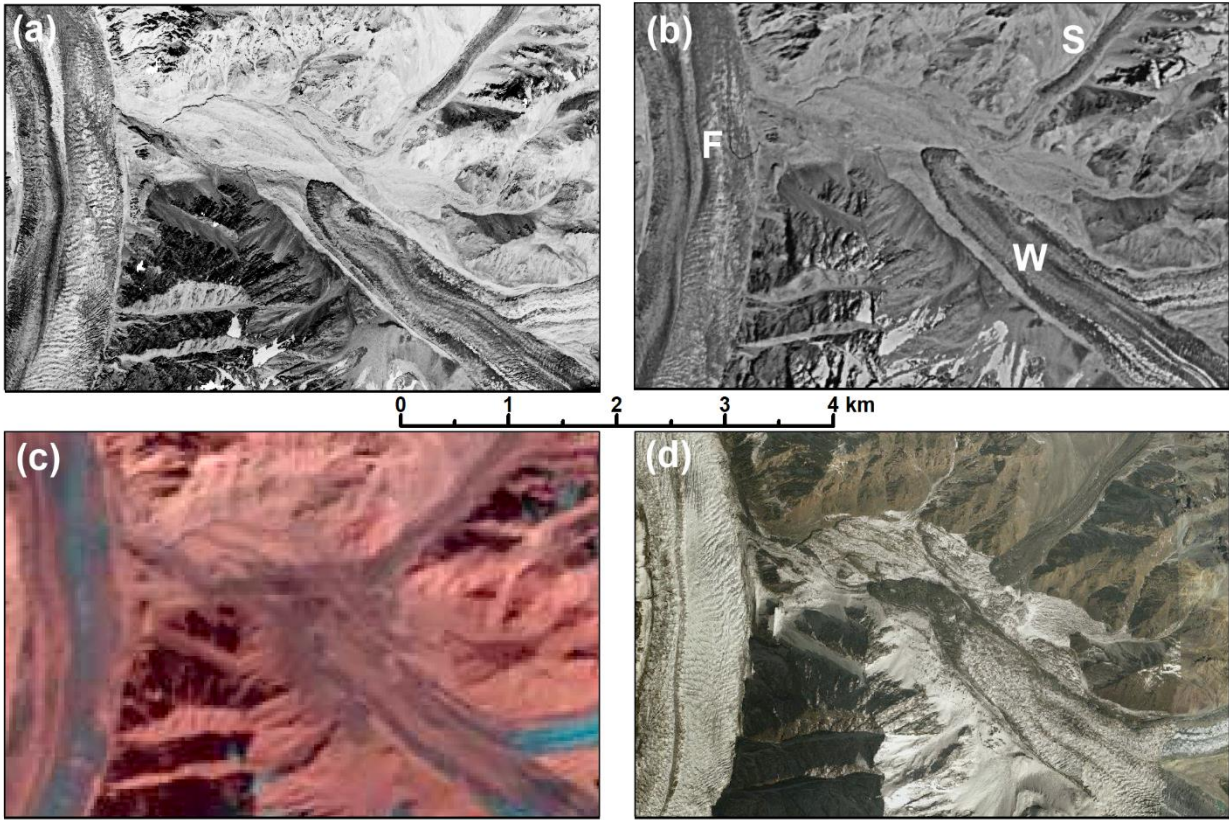
749

750 *Fig. 2: Comparison of satellite images for the same sub-region (see Fig. 1 for location) showing the following*
751 *glaciers: F: Fortambek (18), W: Walter 731 (19), and S: Soldatov (20). The images are acquired by a) Corona in*
752 *1968, b) Hexagon in 1975, c) Landsat in 2017, and d) Bing Maps (date unknown). Image sources: Panels a) to c)*
753 *earthexplorer.usgs.gov, panel d) screenshot from bing.com ©2020 DigitalGlobe.*

754
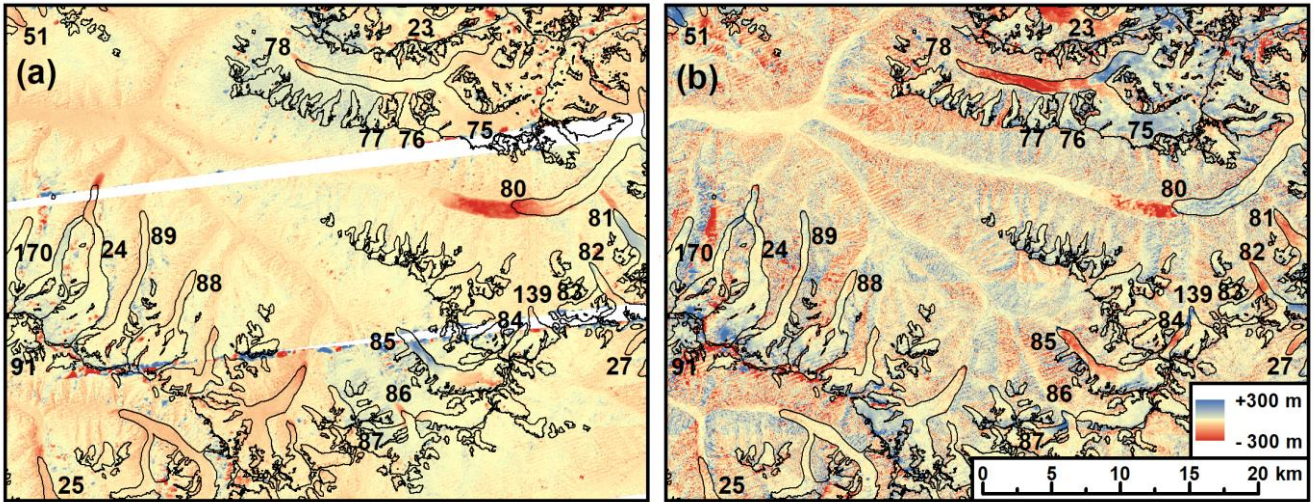
755

756 *Fig. 3: Two examples of colour-coded DEM difference images used to identify surging glaciers (marked with*
757 *their ObjectID). The glacier outlines depict the glacier state at ~2000 (GI-2). A) SRTM-Corona (2000-1968) and*
758 *b) AW3D30-SRTM (~2010-2000).*

759
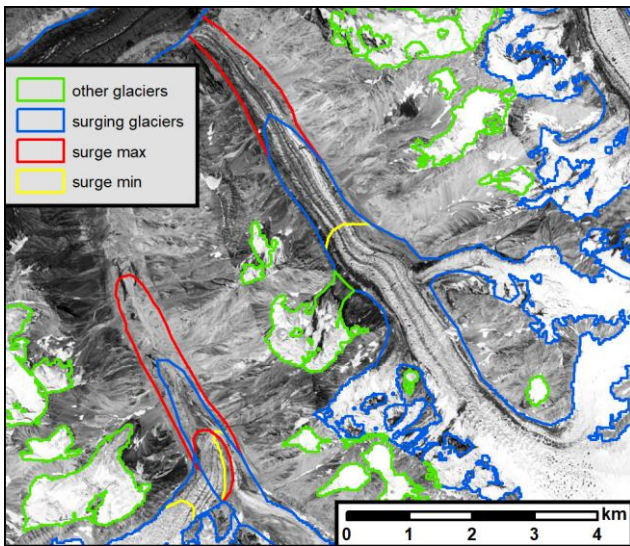
760

761 *Fig. 4: Comparison of glacier outlines from the original inventory GI-2 (blue/green) and the additional GI-3min*
762 */ GI-3max (yellow/red) showing the minimum and maximum extents of two surging glaciers. Image acquisition*
763 *date and source:1968, earthexplorer.usgs.gov.*

764
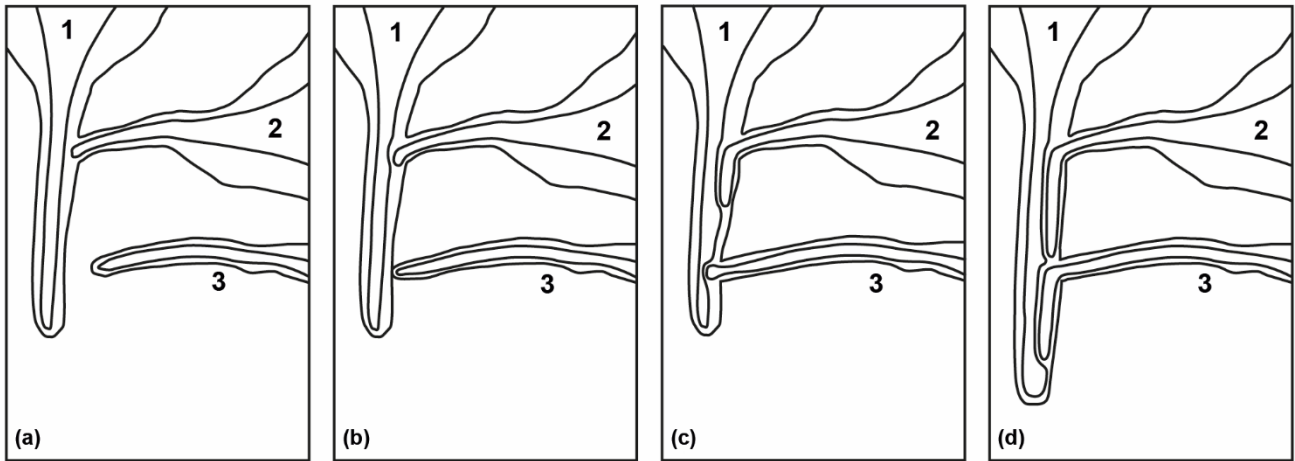
765

766 *Fig. 5: Sketch map of selected possible interactions among surging glaciers of different types. a) At the beginning*
767 *– glacier 2 in full surge mode, b) surge maximum of glacier 2 and surge start of glacier 3, c) surge maximum of*
768 *glacier 3, d) surge of glacier 1. See text for description.*

769
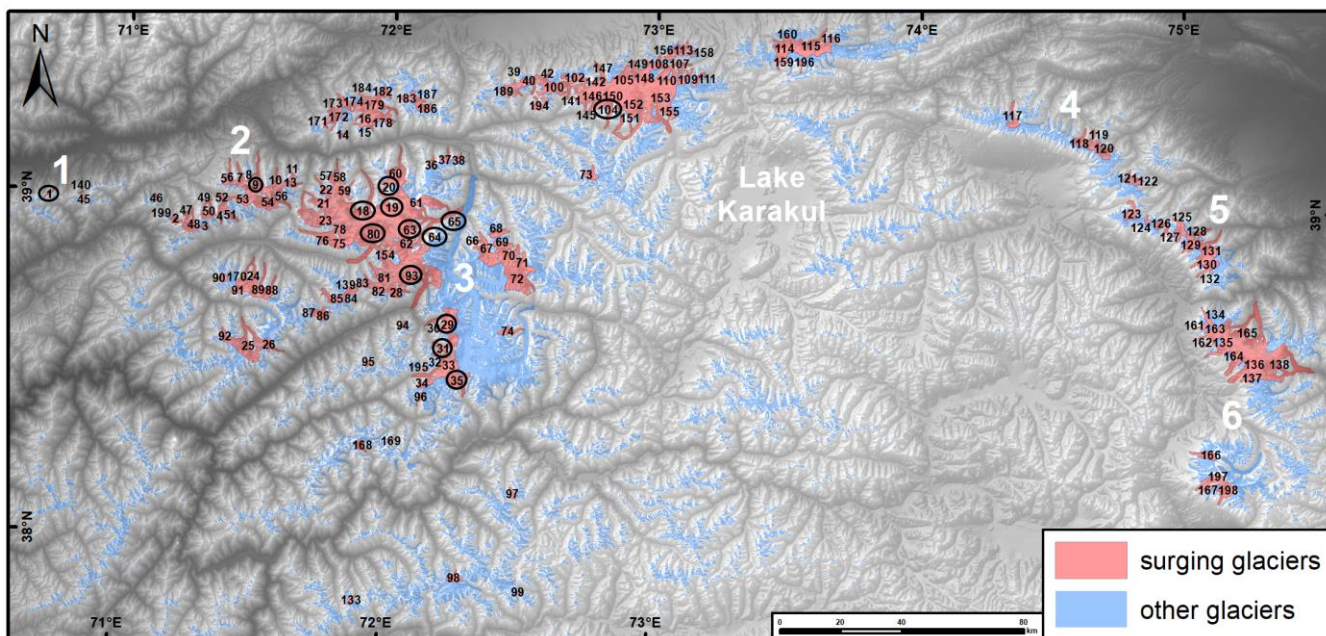
770

771 *Fig. 6: Overview of the identified surging glaciers (red) in the Pamir Mountains. Small black numbers refer to*
772 *their ObjectID in the GI-3min dataset, numbers in circles indicate glaciers mentioned in the text and bold white*
773 *numbers indicate regions mentioned in the text (1 Petr Alervogo West, 2 Petr Alervogo East, 3 Fedchenko, 4*
774 *King Tau, 5 Ulugarttag, 6 Mustagh). DEM source: AW3D30.*

775
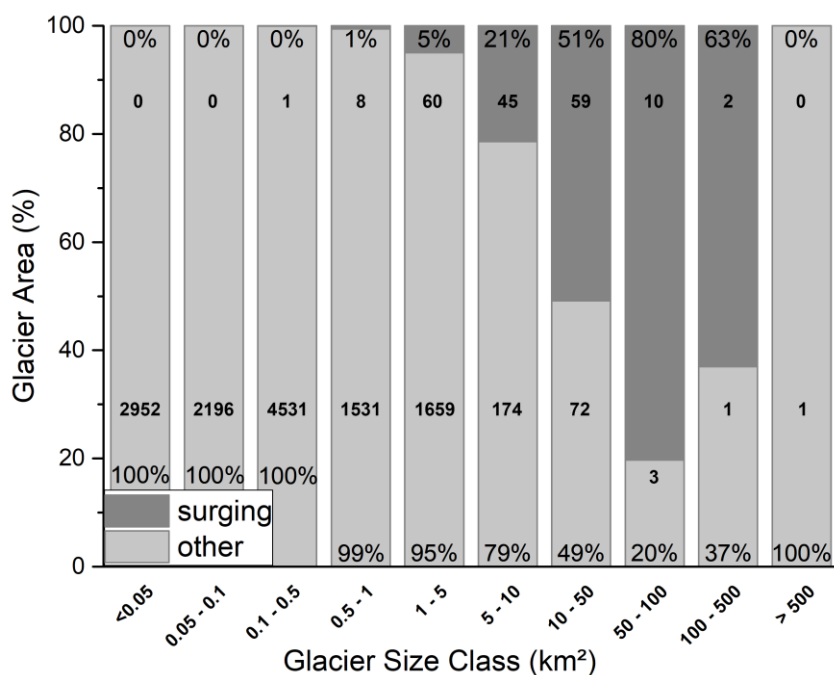
776

777 *Fig. 7: Size class distribution (in relative terms) of surging and other glaciers in GI-2. The upper bold numbers*
778 *provide the count for surge glaciers, the lower one for all other glaciers.*

779
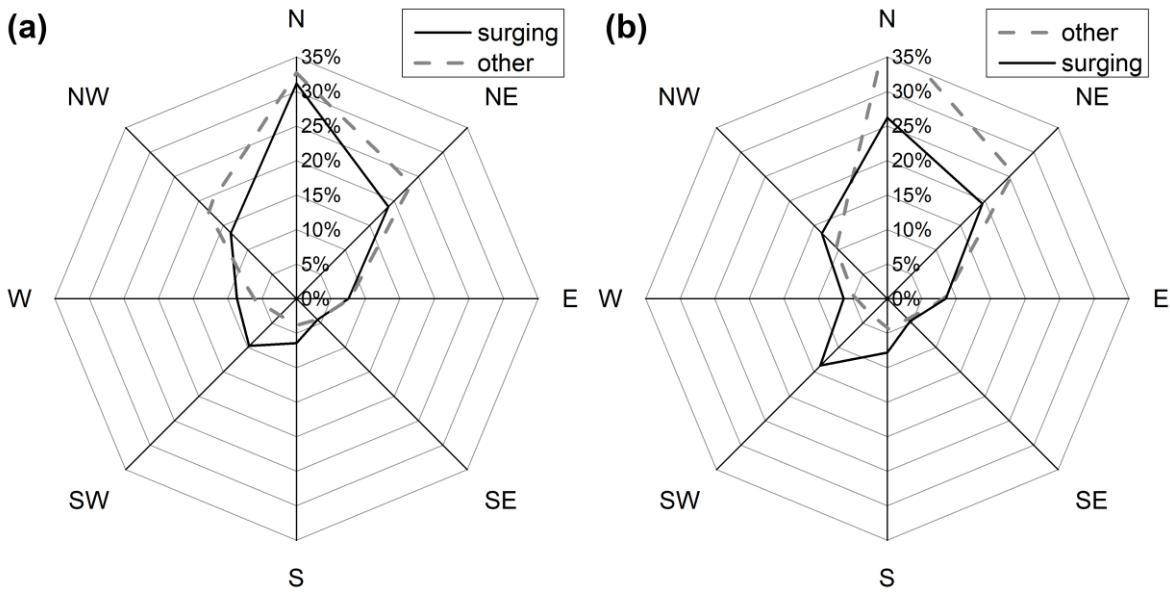
780

781 *Fig. 8: Aspect sector distribution for surging and other glaciers (in relative terms) per a) count and b) area*
782 *covered.*

783
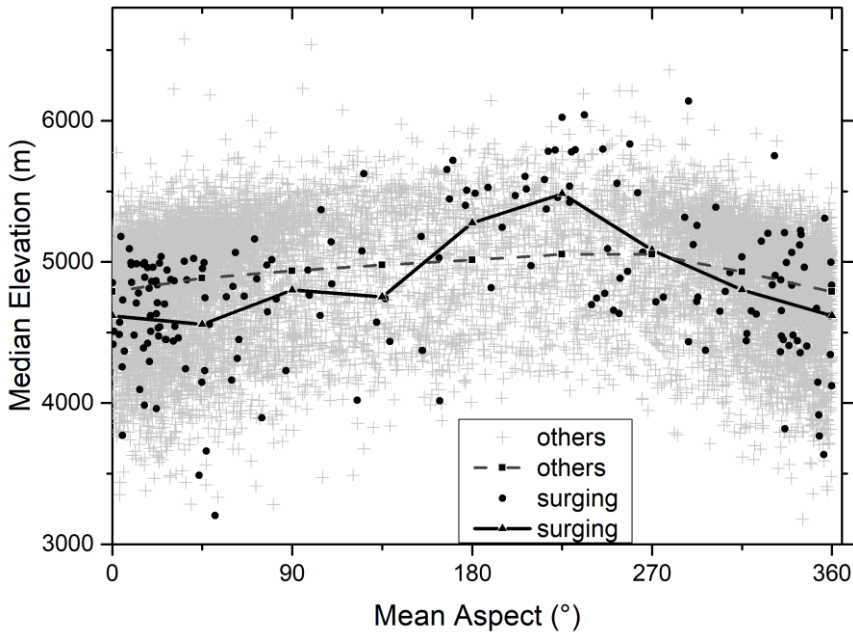
784

785 *Fig. 9: Mean aspect vs. median glacier elevation for surging and other glaciers. The connected lines are*
786 *averages per aspect sector.*

787
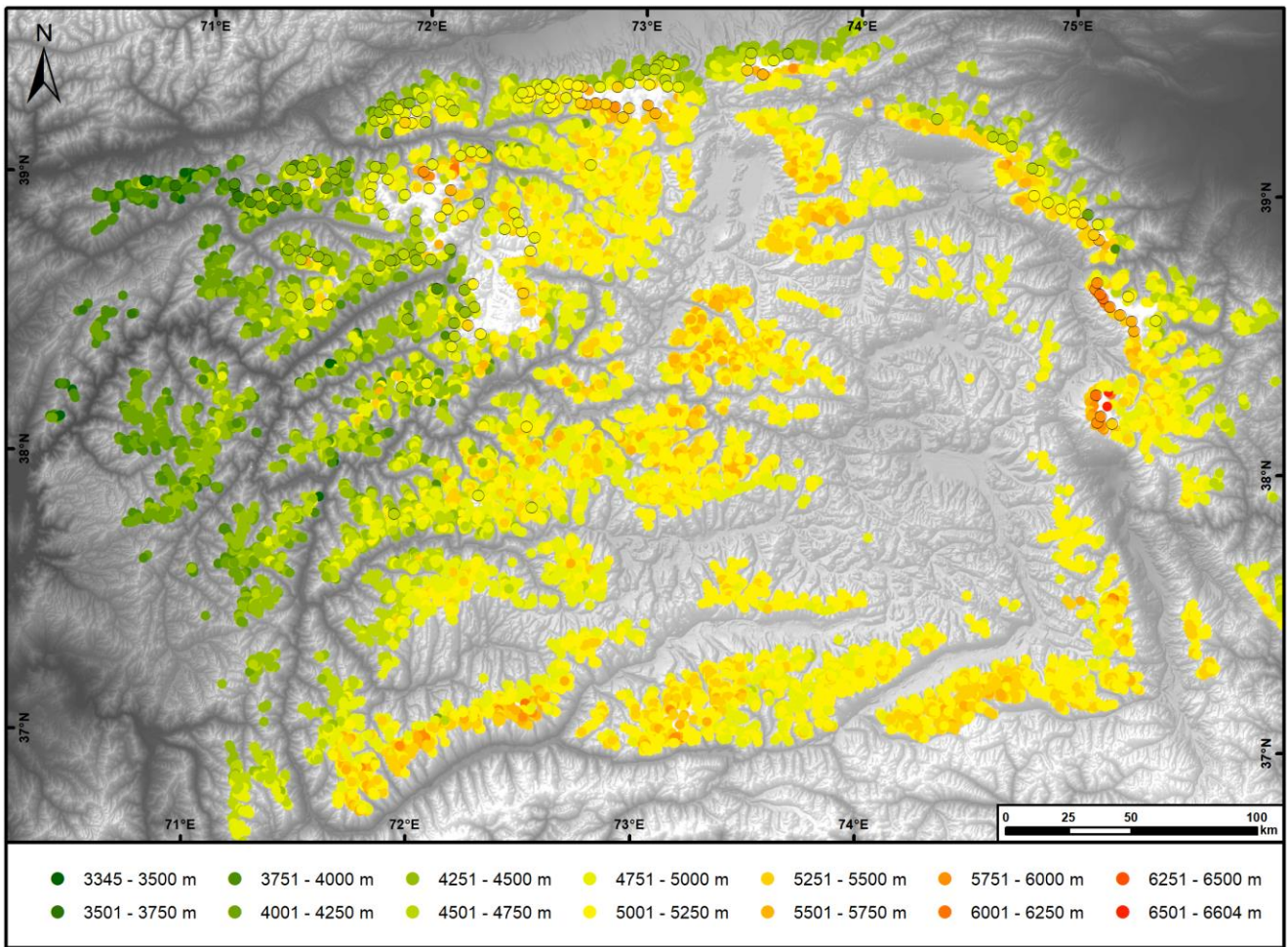
788

789 *Fig. 10: Colour-coded median elevation map with surging glaciers marked (circles with outlines). DEM source:*
790 *AW3D30.*

791

792

793 *Fig. 11: Comparing topographic characteristics of surging glaciers to all others. a) Scatterplot of the elevation*
794 *range vs. glacier size. b) Glacier hypsometry for surging and other glaciers.*

795
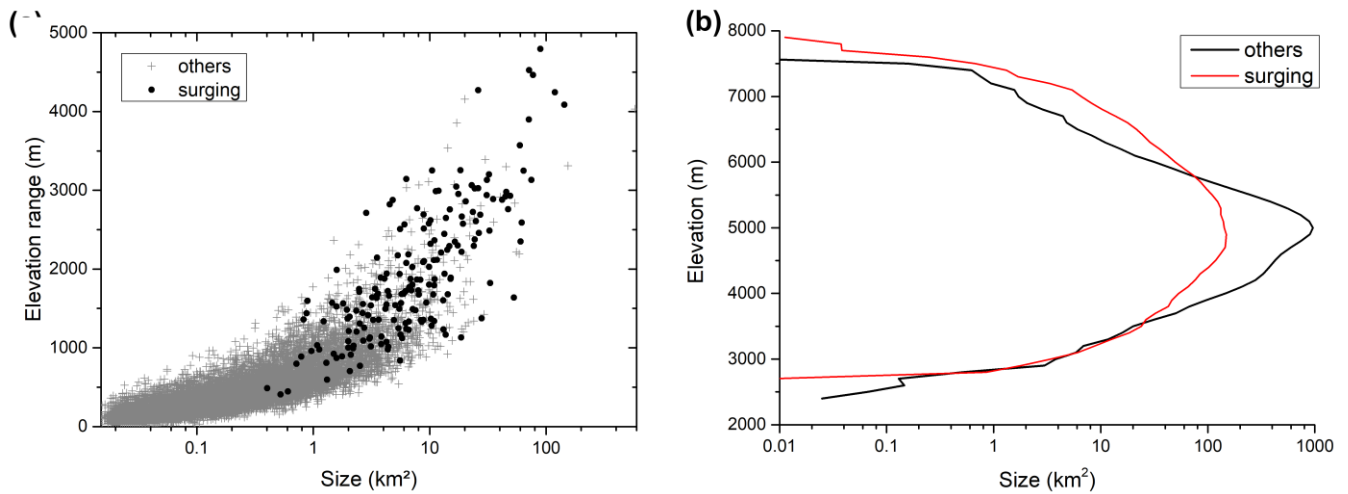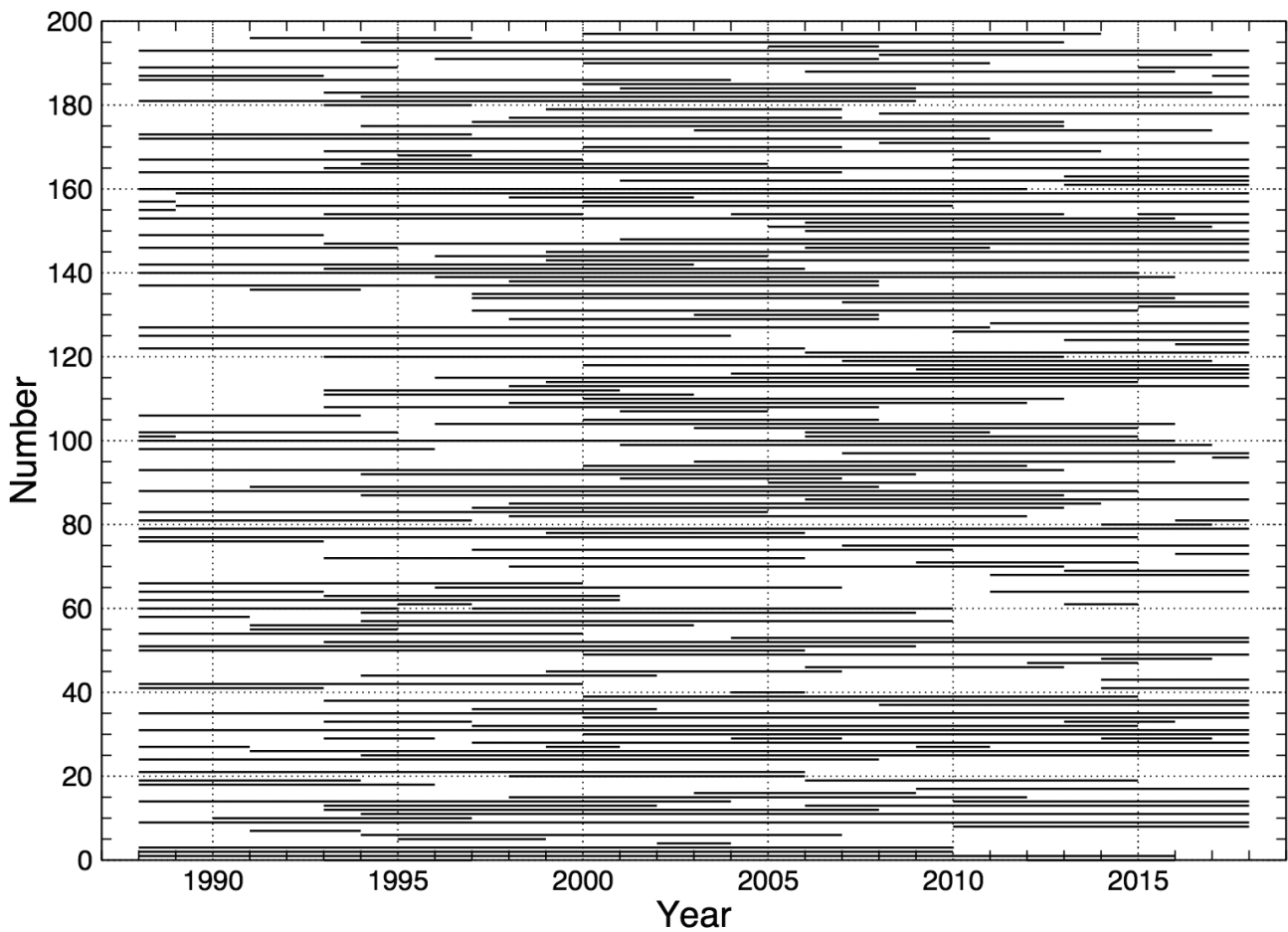
796

797 *Fig. 12: Surge periods for all glaciers with observed surges (GI-3min). Those starting (ending) in 1988 (2018)*
798 *might have started earlier / last longer than indicated by the line.*

799
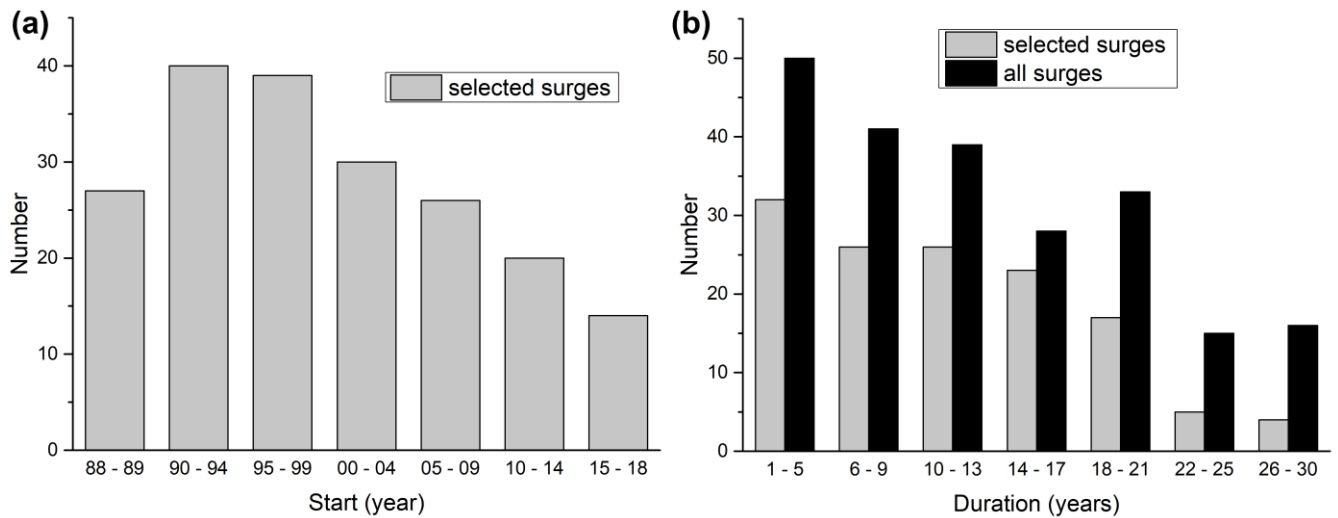
800

801 *Fig. 13: Histograms of surge characteristics. a) Periods in which the surges have started, b) surge durations. The*
802 *charts provide greater detail than the classification code to allow for a better analysis and keep the glacier code*
803 *in the inventory simple. The "88-89" label in a) includes only glaciers that started surging in 1989 as we cannot*
804 *be sure about a surge start of 1988 (might also been earlier). The grey bars in b) refer to the surges that*
805 *occurred completely within the study period, i.e. started after 1988 and ended before 2018.*

806

807